Adaptive motion estimation of a tumbling satellite using laser-vision data with unknown noise characteristics

CONFERENCE PAPER · DECEMBER 2007

DOI: 10.1109/IROS.2007.4399143 · Source: IEEE Xplore

2 AUTHORS, INCLUDING:

F. Aghili
Canadian Space Agency
115 PUBLICATIONS **805** CITATIONS

Proceedings of the 2007 IEEE/RSJ International
Conference on Intelligent Robots and Systems
San Diego, CA, USA, Oct 29 - Nov 2, 2007

Adaptive Motion Estimation of a Tumbling Satellite Using Laser-Vision Data with Unknown Noise Characteristics

Farhad Aghili and Kourosh Parsa
Spacecraft Engineering, Canadian Space Agency
Saint-Hubert, Quebec J3Y 8Y9, Canada
farhad.aghili/kourosh.parsa@space.gc.ca

***Abstract*— A noise-adaptive variant of the Kalman filter is presented for the motion estimation and prediction of a free-falling tumbling satellite as seen from a satellite in a neighboring orbit. A complete dynamics model, including aspects of orbital mechanics, is incorporated for accurate estimation. Moreover, a discrete-time model of the entire system which includes the state-transition matrix and the covariance of process noise are derived effectively in a closed form, which is essential for the real-time implementation of the Kalman filter. We will show that the translational and rotational measurements are coupled and consequently derive the corresponding observation matrix. The statistical characteristics of the measurement noise is formulated by a state-dependent covariance matrix. This model allows additive quaternion noise, while preserving the unit-norm property of the quaternion. The estimator takes the noisy measurements from a laser vision system with unknown and possibly varying statistical noise properties, and subsequently the estimator adaptively estimates the full sates, i.e., the pose and the velocities, in addition to the covariance of the measurement noise and the inertial parameters of the target satellite. Simulations and experiments conducted will demonstrate the quality performance of the adaptive estimator.**

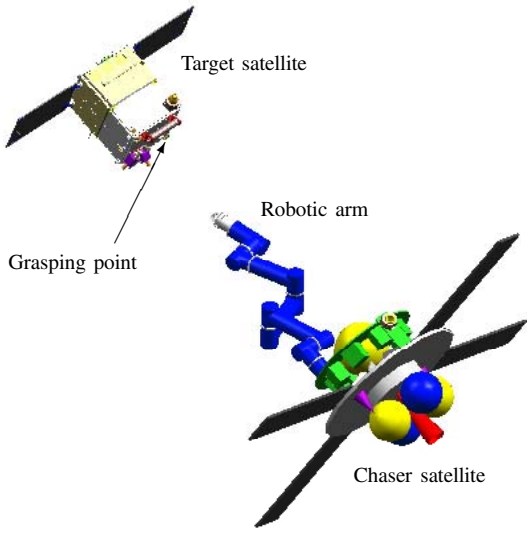

Fig. 1. A chaser satellite trying to capture a target satellite

I. Introduction

Internationally, there has been growing interest in using space robotic systems for the on-orbit servicing of spacecraft [1]–[6]. In such missions, the accurate motion estimation of a free-falling target spacecraft is essential for guiding a robotic arm so as to capture the target. Different vision systems are available for the estimation of the pose (position and orientation) of moving objects. Among them, such an active vision system such as the Neptec Laser Camera system (LCS) is preferable for its robustness in face of the harsh lighting conditions of space [7]. As successfully verified during the STS-105 space mission, the 3D imaging technology used in LCS can indeed operate in space environment. The use of laser range data has also been proposed for the motion estimation of free-floating[1] space objects [8], [9]. All vision systems, however, provide discrete and noisy pose data at relatively low rate, typically 1 Hz, while the capture of a free-falling object is a difficult robotic task which requires real-time and accurate pose estimation.

Taking advantage of the simple dynamics of a free-floating object, researchers have employed different observers to track and predict the motion of a target satellite [8]–[10]. Using a Kalman filter to simultaneously estimate the states and the inertial parameters of a space object was proposed in [8]. In some circumstances, e.g., when there are occlusions, no observation data is available. Therefore, long-term prediction of the motion of the object is needed for planning operations such as autonomous grasping of targets [9], [10].

The Kalman filter uses a dynamics model to compute a rough estimate of the system states, which is then corrected using a model of the sensor measurements to obtain the best estimate possible of the system states based on the present and past measurements. However, the applicability of the Kalman filtering technique rests on the accuracy of the dynamics and the measurement-noise models.

In this work, we use the Euler-Hill equations [11] to derive a discrete-time model that captures the evolution of

[1]It should be noted that, by definition, a *free-falling* object is acted upon by only a gravitational force whereas a *free-floating* object drifts in space with no external force whatsoever. As such, a free-floating object moves at a constant velocity with respect to an inertial frame.

1-4244-0912-8/07/$25.00 ©2007 IEEE.

the relative rotational and translational motions of a tumbling target satellite with respect to a chaser satellite which is free-falling in a nearby orbit. Taking advantage of the structure of the model, we derive numerically efficient expressions for the state transition matrix and the covariance of the process noise, both of which are necessary for the Kalman filter. We also derive the sensitivity matrix of the observation and show that the observations of the translational and rotational displacements are coupled. Moreover, the kinematic properties of the unit-norm quaternions used to represent the relative orientation of the target satellite, is employed to derive the associated measurement-noise covariance. The new model allows *additive* quaternion noise while preserving the unit-norm property of the quaternion. Next, an adaptive variant of the extended Kalman filter (EKF) is used to estimate both the states and the covariance matrix of the measurement noise. This allows autonomous tuning of the filter as the noise characteristics of the vision system change. Finally, the extension of the estimator to the case whereby the moments of inertia of the target tumbling satellite and the location of its center of mass are uncertain is investigated.

II. Modeling

Figure 2 illustrates the chaser and the target satellites as rigid bodies moving in the orbits nearby each other. Coordinate frames $\{\mathcal{A}\}$ and $\{\mathcal{B}\}$ are attached to the chaser and the target, respectively. The origin of $\{\mathcal{B}\}$ is located at the target center of mass (CM) while that of $\{\mathcal{A}\}$ has an offset ρ_c with respect to the CM of the chaser. The axes of $\{\mathcal{B}\}$ are oriented so as to be parallel to the principal axes of the target satellite. Coordinate frame $\{\mathcal{C}\}$ is fixed to the target at its point of reference (POR) located at ρ_t from the origin of $\{\mathcal{B}\}$; it is the pose of $\{\mathcal{C}\}$ which is measured by the laser camera. We further assume that the target satellite tumbles with angular velocity ω. Also, notice that coordinate frame $\{\mathcal{A}\}$ is not inertial; rather, it moves with the chaser satellite. In the following, quantities ρ_t and ω are expressed in $\{\mathcal{B}\}$, while ρ_c is expressed in $\{\mathcal{A}\}$.

The orientation of $\{\mathcal{B}\}$ with respect to $\{\mathcal{A}\}$ is represented by the unit quaternion q. Below, we review some basic definitions and proprieties of quaternions used in the rest of the paper. Consider quaternion q_1, q_2, q_3, and their corresponding rotation matrix R_1, R_2, and R_3. The operators $\otimes$ and $\odot$ are defined as

$$[a\otimes] \triangleq \begin{bmatrix} -\lceil a_v \rceil + a_o I_3 & a_v \\ -a_v^T & a_o \end{bmatrix}, \quad [a\odot] \triangleq \begin{bmatrix} \lceil a_v \rceil + a_o I_3 & a_v \\ -a_v^T & a_o \end{bmatrix},$$

where a_o and a_v are the scalar and vector parts of quaternion a, respectively, and $\lceil a_v \rceil$ is the cross-product matrix of a_v. Then,

$$q_3 = q_1 \otimes q_2 = q_2 \odot q_1,$$

corresponds to product $R_3 = R_1 R_2$. Notice that the quaternion operator matrices $[a\otimes]$ and $[a\odot]$ are analogous to the vector cross product operator matrix $\lceil u \rceil$, which is defined such that $\lceil u \rceil v = u \times v$. Also, the conjugate[2] a^* of a quaternion is defined such that $a^* \otimes a = a \otimes a^* = \begin{bmatrix} 0 & 0 & 0 & 1 \end{bmatrix}^T$.

[2] $a_o^* = a_o$ and $a_v^* = -a_v$.

Assume that quaternion q represent the rotation of the target satellite with resect to the chaser satellite. Then, the relation between the time derivative of the quaternion and the relative angular velocity $\omega_{\rm rel}$ can be elegantly expressed by the following differential equation:

$$\dot{q} = \frac{1}{2}\underline{\omega}_{\rm rel} \otimes q, \tag{1}$$

where

$$\underline{\omega}_{\rm rel} = \begin{bmatrix} \omega_{\rm rel} \\ 0 \end{bmatrix}, \qquad \omega_{\rm rel} = \omega - \omega_n,$$

and ω_n is the angular velocity of the chaser satellite expressed in frame $\{\mathcal{B}\}$. The chaser satellite rotates with the angular velocity of the reference orbit so that it always points towards the Earth center. Assume that $n = \begin{bmatrix} 0 & 0 & n_z \end{bmatrix}^T$ denotes the angular velocity of the reference orbit expressed in $\{\mathcal{A}\}$. Then, one can use the well know transformation by the quaternion of rotation [12] to obtain the angular velocity of the chaser satellite as follows

$$\omega_n = q \otimes \underline{n} \otimes q^* \tag{2}$$

Substituting (2) into (1) and using the properties of quaternion products, we arrive at

$$\dot{q} = \frac{1}{2}\underline{\omega} \otimes q - \frac{1}{2}(q \otimes \underline{n}) \otimes (q^* \otimes q) = \frac{1}{2}\big(\underline{\omega} \otimes -\underline{n} \odot\big) q \tag{3}$$

Consider a small quaternion perturbation

$$\delta q = q \otimes \bar{q}^* \tag{4}$$

Then, adopting a linearization technique similar to [13], [14], one can linearize the above equation about the estimated states $\bar{q}$ and $\bar{\omega}$ to obtain

$$\frac{\mathrm{d}}{\mathrm{d}t}\delta q_v \approx -\bar{\omega}_k \times \delta q_v + \frac{1}{2}\delta\omega \tag{5a}$$

$$\frac{\mathrm{d}}{\mathrm{d}t}\delta q_o \approx 0 \tag{5b}$$

the latter of which, as suggested in [13], can be ignored since δq_o is not an independent variable, and it has variations of only the second order. It is interesting to note that the angular velocity of the chaser satellite does not affect the linearized equation of the time-derivative of the quaternion.

Dynamics of the rotational motion of the target satellite can be expressed by Euler's equation as

$$\dot{\omega} = \psi(\omega) + J\varepsilon_\tau, \quad \text{where} \quad \psi(\omega) = \begin{bmatrix} p_x \omega_y \omega_z \\ p_y \omega_x \omega_z \\ p_z \omega_x \omega_y \end{bmatrix}, \tag{6}$$

where $J = \mathrm{diag}\big(1, I_{xx}/I_{yy}, I_{xx}/I_{zz}\big)$; $p_x = (I_{yy} - I_{zz})/I_{xx}$, $p_y = (I_{zz} - I_{xx})/I_{yy}$, and $p_z = (I_{xx} - I_{yy})/I_{zz}$; I_{xx}, I_{yy}, and I_{zz} are the principal moments of inertia of the target satellite; and ε_τ is a torque disturbance divided by I_{xx}. Linearizing (6) about $\bar{\omega}_k$ yields

$$\frac{\mathrm{d}}{\mathrm{d}t}\delta\omega = A(\bar{\omega})\,\delta\omega + J\varepsilon_\tau, \tag{7}$$

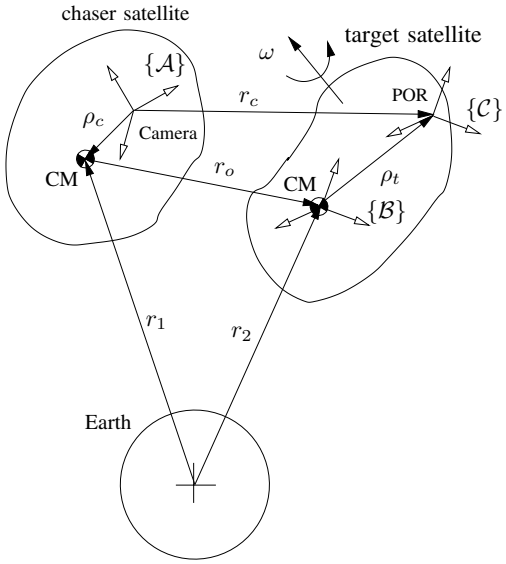

Fig. 2. The body-diagram of chaser and target satellites moving in neighboring orbits

where

$$A(\bar{\omega}) = \left(\frac{\partial \psi}{\partial \omega}\right)_{\omega=\bar{\omega}} = \begin{bmatrix} 0 & p_x\bar{\omega}_{z_k} & p_x\bar{\omega}_{y_k} \\ p_y\bar{\omega}_{z_k} & 0 & p_y\bar{\omega}_{x_k} \\ p_z\bar{\omega}_{y_k} & p_z\bar{\omega}_{x_k} & 0 \end{bmatrix}.$$

Let $x = [q_v^T \;\; \omega^T]^T$ describe the part of the system states pertaining to the rotational motion. Then, from (5a) and (7), we have

$$\frac{\mathrm{d}}{\mathrm{d}t}\delta x = \begin{bmatrix} -\lceil\bar{\omega}_k\rceil & \frac{1}{2}I_3 \\ 0_{3\times3} & A(\bar{\omega}_k) \end{bmatrix}\delta x + \begin{bmatrix} 0_{3\times1} \\ J\epsilon_\tau \end{bmatrix}. \tag{8}$$

The evolution of the relative distance of the two satellites can be described by *orbital mechanics*. Let the chaser move on a circular orbit at an angular rate of n. Further, assume that vector r_o denotes the distance between the CMs of the two satellites expressed in $\{\mathcal{A}\}$, and that $v_o = \dot{r}_o$. Then, if $\{\mathcal{A}\}$ is orientated so that its x-axis is radial and pointing outward, and its y-axis lies on the orbital plane, the translational motion of the target can be expressed as [11], [15]

$$\dot{v}_o = -2n \times v_o + \eta(r_o, n) + \epsilon_f. \tag{9}$$

Here, ϵ_f is the force disturbance for a unit mass, and acceleration term η is due to the effect of orbital mechanics and can be linearized as $\eta^T(r_o, n) \approx [3n_z^2 r_{o_x} \;\; 0 \;\; -n_z^2 r_{o_z}]$. Denoting the states of the translational motion with $y^T = \begin{bmatrix} r_o^T & v_o^T \end{bmatrix}$, one can derive the corresponding dynamics as

$$\frac{\mathrm{d}}{\mathrm{d}t}\delta y = \begin{bmatrix} 0_{3\times3} & I_3 \\ N & -2\lceil n\rceil \end{bmatrix}\delta y + \begin{bmatrix} 0_{3\times1} \\ \epsilon_f \end{bmatrix}. \tag{10}$$

where

$$N \triangleq \frac{\partial \eta}{\partial r_o} = \begin{bmatrix} 3n_z^2 & 0 & 0 \\ 0 & 0 & 0 \\ 0 & 0 & -n_z^2 \end{bmatrix}.$$

III. Discrete Model

A. State Transition Matrix

The discrete-time solutions of the linearized systems (8) and (10) can be written as

$$\delta x_{k+1} = \Phi_{x_k}\delta x_k + \Gamma_{x_k}u_k \tag{11}$$

$$\delta y_{k+1} = \Phi_{y_k}\delta y_k + \Gamma_{y_k}w_k \tag{12}$$

where $\Phi_{x_k} = \Phi_x(t_k; T_\Delta)$ and $\Phi_{y_k} = \Phi_y(t_k; T_\Delta)$ are the *state transition matrices* associated with the system rotational and translational dynamics, respectively, and $T_\Delta = t_{k+1} - t_k$ is the sampling time.

1) Rotational Motion: Assuming $0 \le t \le T_\Delta$ and defining $\varpi_k \triangleq \|\bar{\omega}_k\|$, we can write the state-transition matrix of system (8) as

$$\Phi_{x_k}(t) = \begin{bmatrix} \Phi_{x_{11}}(t) & \Phi_{x_{12}}(t) \\ 0_{3\times3} & \Phi_{x_{22}}(t) \end{bmatrix},$$

where

$$\Phi_{x_{11}}(t) = e^{-\lceil\bar{\omega}_k\rceil t} = I_3 - \frac{\sin\varpi_k t}{\varpi_k}\lceil\bar{\omega}_k\rceil + \frac{1-\cos\varpi_k t}{\varpi_k^2}\lceil\bar{\omega}_k\rceil^2,$$

$$\Phi_{x_{22}}(t) = e^{A(\bar{\omega}_k)t} = \sum_{i=1}^{3}\sum_{j=1}^{3} a_{ij}e^{\lambda_j t}A^{i-1}$$

$$\Phi_{x_{12}}(t) = \frac{1}{2}\sum_{i=1}^{3}\sum_{j=1}^{3}\sum_{k=1}^{3}\gamma_{ij}\phi_{jk}\lceil\bar{\omega}_k\rceil^{k-1}A^{i-1} \tag{13}$$

In the above, λ_is are the distinct eigenvalues of matrix A, and γ_{ij}s can be constructed from the eigenvalues as described in Appendix A, and scalar functions $\phi_{kj}(t)$s are calculated from

$$\phi_{j1}(t) = \lambda_j^{-1}(e^{\lambda_j t} - 1),$$

$$\phi_{j2}(t) = (\lambda_j^2\varpi_k + \varpi_k^3)^{-1}\big(\varpi_k\cos\varpi_k t + \lambda_j\sin\varpi_k t - e^{\lambda_j t}\varpi_k\big),$$

$$\phi_{j3}(t) = \varpi_k^{-2}\lambda_j^{-1} + (\lambda_j^3\varpi_k^2 + \lambda_j\varpi_k^4)^{-1}\big(\lambda_j^2\cos\varpi_k t - \varpi_k\lambda_j\sin\varpi_k t + \varpi_k^2 e^{\lambda_j t}\big).$$

2) Translational Motion: Writing the Taylor expansion of the state-transition matrix of the translational system (10) about $n = 0$, we get

$$\Phi_{y_k}(t) = \begin{bmatrix} I_3 & \Phi_{y_{12}}(t) \\ 0_{3\times3} & \Phi_{y_{22}}(t) \end{bmatrix} + \mathcal{O}(n^2), \tag{14}$$

where

$$\Phi_{y_{12}}(t) = \begin{bmatrix} t & n_z t^2 & 0 \\ 0 & t & 0 \\ 0 & 0 & t \end{bmatrix} \quad \text{and} \quad \Phi_{y_{22}}(t) = I_3 - 2\lceil n\rceil t.$$

Since $n_z t$ for $0 \le t \le T$ has a small value, we neglect the second- and higher-order terms in (14).

B. Covariance Matrix of Process Noise

In our model, the effects of flexible appendages (such as solar panel), gravity gradient, and fuel sloshing are not considered because, in practice, it is usually sufficient to model them as process noise in the Kalman filter [8]. Presumably, the continuous process noise is with covariances

$\Sigma_\tau = E[\epsilon_\tau \epsilon_\tau^T] = \sigma_\tau^2 I_3$ and $\Sigma_f = E[\epsilon_f \epsilon_f^T] = \sigma_f^2 I_3$. Let $Q_k = \text{diag}(Q_{x_k}, Q_{y_k})$, where Q_{x_k} and Q_{y_k} are covariance matrices of the discrete-time process noise pertaining to the rotational and the translational systems, respectively. In turn, Q_{x_k} can be calculated from

$$Q_{x_k} = \Gamma_{x_k} E[u_k u_k^T] \Gamma_{x_k}^T = \int_0^T \Phi_{x_k}(t) G_k \Sigma_\tau G_k^T \Phi_{x_k}^T(t)\, \mathrm{d}t \tag{15}$$

with $G_k^T = \begin{bmatrix} 0_{3\times 3} & J^T \end{bmatrix}$, thus resulting in

$$Q_{x_k} = \sigma_\tau^2 \int_0^T \begin{bmatrix} Q_{x_{11}} & Q_{x_{12}} \\ Q_{x_{12}} & Q_{x_{22}} \end{bmatrix} \mathrm{d}t$$

where

$$Q_{x_{11}} = \frac{1}{4}\Phi_{x_{12}} J^2 \Phi_{x_{12}}^T, \quad Q_{x_{12}} = \frac{1}{2}\Phi_{x_{12}} J^2 \Phi_{x_{22}}^T, \quad Q_{x_{22}} = \Phi_{x_{22}} J^2 \Phi_{x_{22}}^T. \tag{16}$$

After integration of the state-transition matrix (15) and truncating the third-order terms and higher, we arrive at

$$Q_{y_k} = \Gamma_{y_k} E[w_k w_k^T] \Gamma_{y_k}^T = \sigma_f^2 \begin{bmatrix} Q_{y_{11}} & Q_{y_{12}} \\ Q_{y_{12}} & Q_{y_{22}} \end{bmatrix} + \mathcal{O}(n^3).$$

where

$$Q_{y_{11}} = \begin{bmatrix} \frac{1}{3}T_\Delta^3 + \frac{2}{5}n_z^2 T_\Delta^5 & \frac{1}{4}(n_z - n_z^2)T_\Delta^4 & 0 \\ \frac{1}{4}(n_z - n_z^2)T_\Delta^4 & \frac{1}{3}T_\Delta^3 - \frac{4}{15}n_z^2 T_\Delta^5 & 0 \\ 0 & 0 & \frac{1}{3}T_\Delta^3 - \frac{1}{15}n_z^2 T_\Delta^5 \end{bmatrix},$$

$$Q_{y_{12}} = \begin{bmatrix} \frac{1}{2}T_\Delta^2 + \frac{1}{3}n_z^2 T_\Delta^4 & -\frac{1}{3}n_z T_\Delta^3 & 0 \\ \frac{2}{3}(n_z - n_z^2)T_\Delta^3 & \frac{1}{2}T_\Delta^2 - \frac{2}{3}n_z^2 T_\Delta^4 & 0 \\ 0 & 0 & \frac{1}{2}T_\Delta^2 - \frac{1}{6}n_z^2 T_\Delta^4 \end{bmatrix}$$

$$Q_{y_{22}} = \begin{bmatrix} T_\Delta + n_z^2 T_\Delta^3 & 0 & 0 \\ 0 & T_\Delta & 0 \\ 0 & 0 & T_\Delta - \frac{1}{3}n_z^2 T_\Delta^3 \end{bmatrix}.$$

C. Observation Matrix

The vision system, namely, the LCS, measures both the orientation of $\{\mathcal{C}\}$ and the position vector r_c of its origin in the LCS frame. Apparently, we have

$$r_c = \rho_c + r_o + R(q)\rho_t, \tag{17}$$

where the rotation matrix $R(q)$ from $\{\mathcal{B}\}$ to $\{\mathcal{A}\}$ is obtained from the quaternion as

$$R(q) = (2q_o^2 - 1)I + 2q_o \lceil q_v \rceil + 2q_v q_v^T \tag{18}$$

To write the linearized observation relation, the variation of the LCS measurements, namely, r_c and q, with respect to their nominal values, namely, $\bar{r}_c$ and $\bar{q}$, are taken. Then, for the orientation part, we choose the vector part of the quaternion representing the orientation variation, i.e., $\delta q_v = \big(q \otimes \bar{q}^*\big)_v$ with $(\cdot)_v$ denoting the vector part of a quaternion. Thus, the observation vector becomes

$$z = h(x) + \begin{bmatrix} v_1 \\ v_2 \end{bmatrix}, \tag{19}$$

where v_1 and v_2 are additive measurement noise processes and

$$h(x) \triangleq \begin{bmatrix} r_c - \bar{r}_c \\ \delta q_v \end{bmatrix}. \tag{20}$$

To implement the filter, one needs to derive the sensitivity of z with respect to the system states. Because $q = \delta q \otimes \bar{q}$, in view of (17), we will have

$$\begin{aligned} r_c - \bar{r}_c &= r_o + R(\delta q \otimes \bar{q})\rho_t - \bar{r}_o - R(\bar{q})\rho_t \\ &= \delta r_o + R(\bar{q})\big(R(\delta q) - I_3\big)\rho_t \end{aligned} \tag{21}$$

in which we have used the identity $R(q_1 \otimes q_2) \equiv R(q_2)\, R(q_1)$. Then, it can readily be seen from (18) that, for a small rotation δq, i.e., $\|\delta q_v\| << 1$ and $\delta q_0 \approx 1$, we have

$$R(\delta q) \approx I_3 + 2\lceil \delta q_v \rceil.$$

Hence, (19) can be approximated as

$$z = \begin{bmatrix} z_1 \\ z_2 \end{bmatrix} = \begin{bmatrix} \delta r_o - 2R(\bar{q})(\rho_t \times \delta q_v) \\ \delta q_v \end{bmatrix} + v$$

where $v^T \triangleq [v_1^T \; v_2^T]$. Therefore, the linearized measurement equation and the sensitivity matrix are obtained as

$$z_k = H_k \delta x_k + v_k, \tag{22a}$$

$$H_k = \begin{bmatrix} -2R(\bar{q}_k)\lceil \rho_t \rceil & 0_{3\times 3} & I_3 & 0_{3\times 3} \\ I_3 & & 0_{3\times 9} & \end{bmatrix}. \tag{22b}$$

D. Propagation of Measurement Noise

The challenge in modeling the quaternion error in the form of additive noise is that the unit-norm property of the quaternion must be preserved. That imposes a constraint on the additive noise, thus leading to a state-dependent covariance matrix, as seen below. Assume that $q_m = q + \epsilon_q$ be the unnormalized measured variable that contains small noise ϵ_{q_m}. Then, a valid measurement z_2 can be obtained by a simple normalization of the q_m as

$$\begin{aligned} z_2 &= \big(\bar{q}^* \odot \frac{q + \epsilon_q}{\|q + \epsilon_q\|}\big)_v \\ &\approx \delta q_v + \Big(\bar{q}^* \odot \frac{\partial}{\partial \epsilon_q}\Big(\frac{q_m + \epsilon_q}{\|q_m + \epsilon_q\|}\Big)\Big|_{\epsilon_q = 0} \epsilon_q\Big)_v \\ &= \delta q_v + \big(\bar{q}^* \odot \epsilon_q\big)_v - \big(\delta q_v \delta q^T (\bar{q} \otimes \epsilon_q)\big)_v. \end{aligned} \tag{23}$$

Neglecting the second order term, i.e., $\delta q \delta q^T$, in (23), we can write the latter equation as

$$z_{2_k} = \delta q_{v_k} + T(\bar{q}_k)\epsilon_q \tag{24}$$

where $T(\bar{q}_k) = [\lceil \bar{q}_{v_k} \rceil - \bar{q}_{o_k} I_3 \;\; \bar{q}_{v_k}]$. Therefore, the covariance of the orientation noise can be computed from

$$\begin{aligned} E[v_{2_k} v_{2_k}^T] = &-\lceil \bar{q}_{v_k} \rceil \Sigma_{q_v} \lceil \bar{q}_v \rceil + \bar{q}_{o_k}\big(\Sigma_{q_v}\lceil \bar{q}_{v_k}\rceil - \lceil \bar{q}_{v_k}\rceil \Sigma_{q_v}\big) \\ &+ \bar{q}_{v_k}\bar{q}_{v_k}^T \sigma_{q_o}^2 \end{aligned}$$

Note that in the case of homogeneous orientation noise, i.e., $\Sigma_{q_v} = \sigma_{q_o}^2 I_3$, the equation of the covariance is drastically reduced to $E[v_2 v_2^T] = \sigma_{q_o}^2 I_3$.

E. Filter design

In order to take into account the composition rule of quaternion, the states to be estimated by the Kalman filter have to be defined as $\hat{\chi}^T \triangleq [\delta\hat{q}_v^T \ \hat{\omega}_k^T \ \hat{r}_o^T \ \hat{v}_o^T]$. Therefore, one can combine the nonlinear equations (6), (9) and the variation version of (3) in the standard form as $\dot{\chi} = f(\chi, \epsilon)$, where $\epsilon^T = [\epsilon_\tau^T \ \epsilon_f^T]$.

Recall that δq_v is a small deviation from the the nominal trajectory $\bar{q}$. Since the nominal angular velocity $\bar{\omega}_k$ is assumed constant during each interval, the trajectory of the nominal quaternion can be obtained from

$$\bar{q}(t) = e^{\frac{1}{2}(t-t_0)\underline{\bar{\omega}}_k \otimes} \bar{q}(t_0) \quad \Longrightarrow \quad \bar{q}_k = e^{\frac{1}{2}T\underline{\hat{\omega}}_{k-1} \otimes} \hat{q}_{k-1}$$

The EKF-based observer for the associated noisy discrete system (11) is given in two steps: (i) estimate correction

$$K_k = P_k^- H_k^T \big(H_k P_k^- H_k^T + S_k\big)^{-1} \tag{25a}$$
$$\hat{\chi}_k = \hat{\chi}_k^- + K\big(z_k - h(\hat{\chi}_k^-)\big) \tag{25b}$$
$$P_k = \big(I - K_k H_k\big) P_k^- \tag{25c}$$

and (ii) estimate propagation

$$\hat{\chi}_{k+1}^- = \hat{\chi}_k + \int_{t_k}^{t_{k+1}} f(\chi(t), 0)\, \mathrm{d}t \tag{26a}$$
$$P_{k+1}^- = \Phi_k P_k \Phi_k^T + Q_k \tag{26b}$$

and the body orientation is computed from

$$\hat{q}_k = \delta\hat{q}_k \otimes \bar{q}_k$$

right after the innovation step (25b) as

$$\hat{q}_k = \begin{bmatrix} \delta\hat{q}_{v_k} \\ \big(1 - \|\delta\hat{q}_{v_k}\|^2\big)^{\frac{1}{2}} \end{bmatrix} \otimes e^{\frac{1}{2}T_\Delta[\underline{\hat{\omega}}_{k-1} \otimes]} \hat{q}_{k-1}$$

IV. Adaptive Estimator

A. Noise-Adaptive Filter

In a noise-adaptive Kalman filters, the estimation problem is that, in addition to the states, the covariance matrix S_k of the measurement noise v_k has to be estimated. We adopt the batch-processing approach for estimation of the covariance matrix [16], [17] to design a recursive one.

To that end, let us define

$$e_k \triangleq z_k - H_k\hat{\chi}_k^- = H_k(\hat{\chi}_k - \hat{\chi}_k^-) + v_k,$$

which, in fact, is a zero-mean, white noise sequence. Taking the covariances of the both sides of the above equation yields

$$W_k \triangleq E[e_k e_k^T] = H_k P_k^- H_k^T + S_k.$$

Therefore, an estimate of S_k can be obtained from

$$\hat{S}_k = \hat{W}_k - H_k P_k^- H_k^T$$

where

$$\hat{W}_k = \frac{1}{k}\sum_{i=1}^{k} \tilde{e}_i \tilde{e}_i^T, \quad \text{where} \quad \tilde{e}_i = e_i - \bar{e}_i, \tag{27}$$

with $\bar{e}_i = \frac{1}{i}\sum_{j=1}^{i} e_j$ being the statistical sample mean. It can be shown that the batch processing (27) is equivalent to this recursive formulation:

$$\tilde{e}_k = \frac{k-1}{k}\tilde{e}_{k-1} + \frac{k-1}{k}\big(e_k - e_{k-1}\big) \tag{28a}$$
$$\hat{W}_k = \frac{k-1}{k}\hat{W}_{k-1} + \frac{1}{k}\tilde{e}_k\tilde{e}_k^T. \tag{28b}$$

Clearly, the dynamics equation (28b) preserves the positive definiteness of $\hat{W}_k$ if it is appropriately initialized. Thereafter, $\hat{W}_k^{-1}$ remains well defined for all k.

B. Uncertain Inertial and Kinematic Parameters

The pose estimation problem can be extended for the case where not only the inertia of target satellite but also the location of its CM are uncertain. Let vector

$$\theta = \begin{bmatrix} p \\ \rho_t \end{bmatrix}$$

contain the unknown inertial parameters, where $p^T = \big[p_x \quad p_y \quad p_z\big]$. Analogous to (7), linearizing the dynamic equation about $\bar{\omega}_k$ and $\bar{p}$ yields

$$\frac{\mathrm{d}}{\mathrm{d}t}\delta\omega = A(\bar{\omega}_k, \bar{p})\delta\omega + B(\bar{\omega}_k)\delta p + J\varepsilon_\tau, \tag{29}$$

where

$$B(\omega) \triangleq \frac{\partial\psi}{\partial p} = \mathrm{diag}\begin{bmatrix}\omega_y\omega_z & \omega_x\omega_z & \omega_x\omega_y\end{bmatrix}.$$

Define the augmented states of the rotational system as $x'^T \triangleq \big[x^T \quad \theta^T\big]$. Since θ is a constant vector, it seems quite natural to describe the dynamics associated with the parameters simply by $\theta_{k+1} = \theta_k$,. However, it is known that if the unknown parameter vector θ is considered to be deterministic, then it cannot be identified via the extended Kalman filtering technique [16]. This is because Kalman filter becomes overconfident on the model in the absence of process noise, and consequently it does not incorporate the measurement in the estimation process. Therefore, in order that to allow the estimated parameters to be affected by the measurement, θ must be treated as random constant vector as

$$\theta_{k+1} = \theta_k + \zeta_k, \tag{30}$$

where ζ_k is a fictional zero-mean Gaussian white noise sequence, e.g., $E[\zeta\zeta^T] = \mathrm{diag}\{\sigma_p^2 I_3, \sigma_{\rho_t}^2 I_3\}$.

Now integrating (29) and (30), we obtain the state transition matrix of the new system as

$$\Phi_{x_k}(t) = \begin{bmatrix} \Phi_{x_k}(t) & \begin{bmatrix}\Phi_{x_{13}}(t) & 0_{3\times3}\\ \Phi_{x_{23}}(t) & 0_{3\times3}\end{bmatrix} \\ 0_{6\times6} & I_6 \end{bmatrix},$$

where

$$\Phi_{x_{13}}(t) = \sum_{i=1}^{3}\sum_{j=1}^{3} a_{ij}\lambda_j^{-1}\big(e^{\lambda_j t} - 1\big)A^{i-1}B,$$

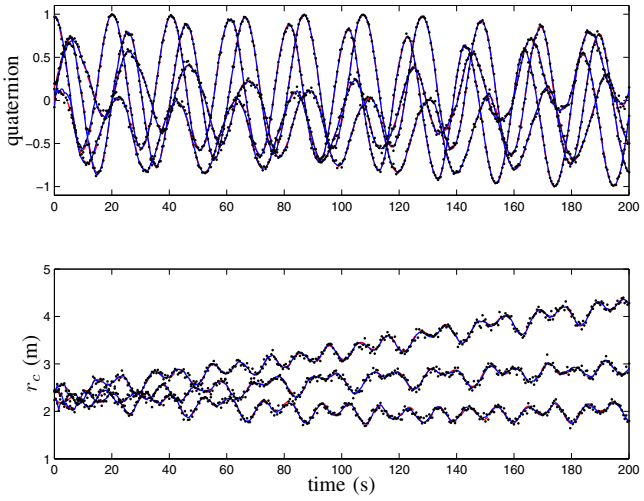

Fig. 3. The estimated pose (solid lines) verse the measured (dotted lines) and the actual ones (dashed lines)

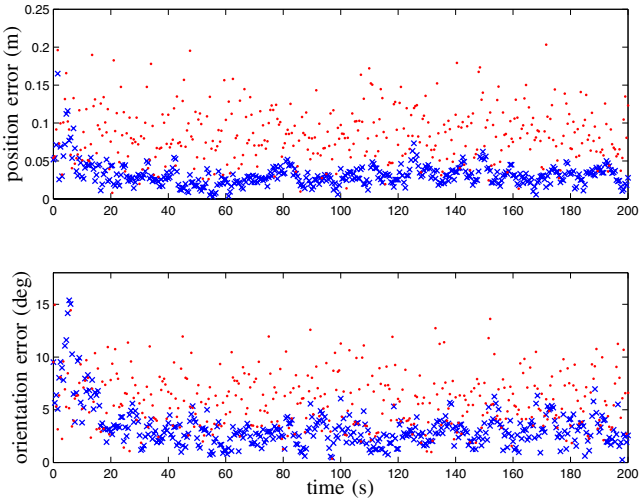

Fig. 4. The error in measured (dot) and estimated (cross) pose

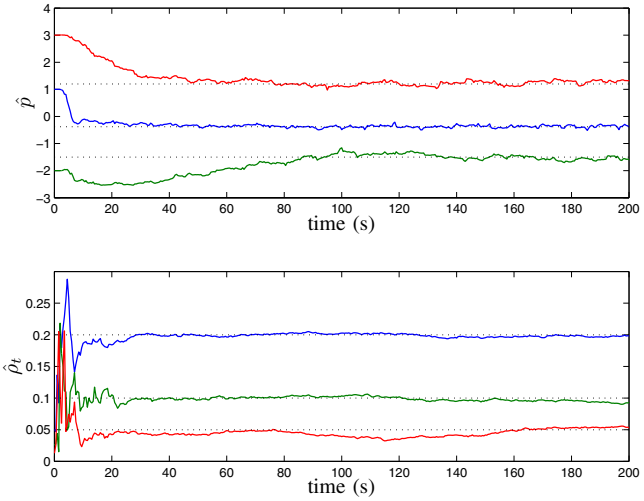

Fig. 5. Convergence of the estimated parameters

and $\Phi_{x_{23}}(t) = \Phi'_{x_{12}} B$, where matrix $\Phi'_{x_{12}}$ can be obtained from polynomial (13) if the scalar functions $\phi_{kj}(t)$s are replaced by

$$\begin{aligned}
\phi'_{1j}(t) &= \lambda_j^{-2}\big(1 - e^{\lambda_j t}\big) - \lambda_j^{-1} t,\\
\phi'_{2j}(t) &= (\lambda_j^3 \varpi_k^2 + \lambda_j \varpi_k^4)^{-1}\big(\varpi_k \lambda_j \sin \varpi_k t + \lambda_j^2 \cos \varpi_k t\\
&\quad + \varpi_k^2 e^{\lambda_j t} - \lambda_j^2 - \varpi_k^2\big),\\
\phi'_{3j}(t) &= \varpi_k^{-2}\lambda_j^{-2} + (\lambda_j^4 \varpi_k^3 + \lambda_j^2 \varpi_k^5)^{-1}\big(\lambda_j^3 \sin \varpi_k t\\
&\quad - \varpi_k \lambda_j^2 \cos \varpi_k t - \varpi_k^3 e^{-\lambda_j t} - (\varpi_k^3 \lambda_j + \lambda_j^3 \varpi_k) t\big).
\end{aligned}$$

Moreover, because

$$\frac{\partial z_1}{\partial \rho_t} = R(q),$$

a development similar to (22a) yields

$$H'_k = \begin{bmatrix} -2R(\bar{q})\lceil \bar{\rho}_t \rceil & 0_{3\times 6} & R(\bar{q}) & I_3 & 0_{3\times 3} \\ & I_3 & 0_{3\times 15} & & \end{bmatrix}. \quad (31)$$

The discrete-time covariance matrix of the augmented system can be obtained from a development analogous to (15). However, it should ne noted G_k is no longer a constant matrix. This is because the inverse of the inertia matrix J has to be calculated from the estimated parameters through

$$\hat{J}_k = \mathrm{diag}\big(1,\ \frac{1-\bar{p}_{y_k}}{1+\bar{p}_{x_k}},\ \frac{1+\bar{p}_{z_k}}{1-\bar{p}_{x_k}}\big).$$

V. Simulation

The convergence property of the adaptive Kalman filter has been investigated through simulations, and the results are presented in this section. The target satellite is assumed to have known inertial properties $I = \mathrm{diag}\begin{bmatrix}4 & 8 & 5\end{bmatrix}$ kgm^2 and $\rho_t = \begin{bmatrix}0.2 & 0.1 & 0.05\end{bmatrix}^T$ m. It is further assumed that the target and the chaser satellites traverse in circular orbits with an angular velocity $n = 0.07$ deg/s. In our simulations, the vision system is affected by measurement noise process with statistical values $\sigma_r = 0.003 I_3$ m^2 and $\sigma_\varphi = 0.001 I_3$ deg^2, which are not known by the estimator; rather, our estimator begins with initial values which are off the true covariances with considerable errors of 100%.

The trajectories of the actual and estimated poses as well as the measured and the actual ones are depicted in Fig. 3. The measured and estimated pose errors are shown in Fig. 4. Here, the errors are simply measured by

$$\begin{aligned}
\text{position error} &= \|r_c - r_{c_{\mathrm{act}}}\|,\\
\text{orientation error} &= 2\sin^{-1}\|\big(q_{\mathrm{act}} \otimes q^*\big)_v\|,
\end{aligned}$$

where $r_{c_{\mathrm{act}}}$ and q_{act} are the actual distance and the actual quaternion, respectively. Finally, Figs. 5 and 6 illustrate the time-history of the estimated parameters and the diagonal elements of the estimated covariance matrices associated with the translational and orientation measurement-noise processes.

VI. Experiment

In this section experimental results are presented that show the performance of the adaptive predictor to provide a 20s

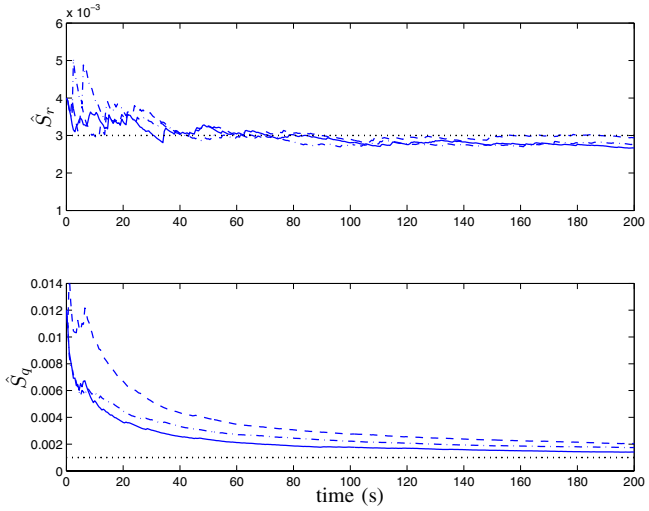

Fig. 6. Convergence of the estimated measurement noise covariance.

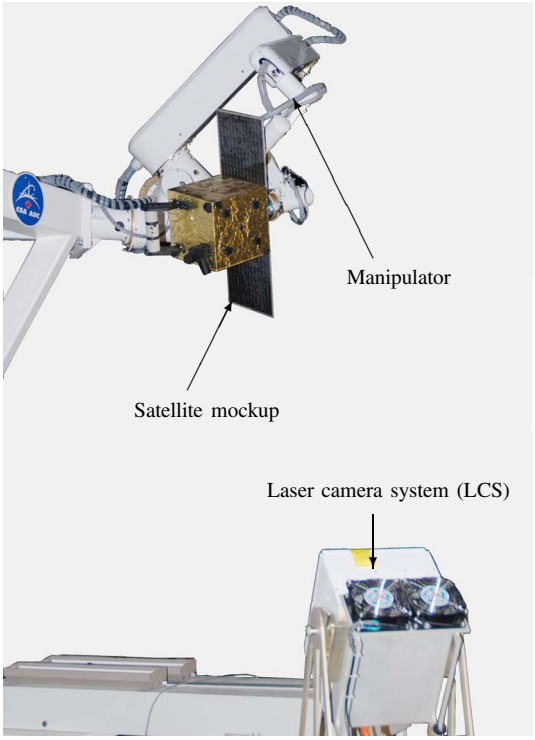

Fig. 7. The experimental setup

ahead of time prediction of the pose trajectory of a satellite based on the estimate of the full states and parameters at a given time. The Neptec Laser Camera system (LCS) [7], is used to obtain the pose measurements at a rate of 2Hz. *A priori* knowledge about neither the inertial and CM of the target satellite nor the noise property of the vision sensor is given to the predictor. Fig. 7 illustrates the experimental setup, whereby the mockup of a satellite is moved by a manipulator according to orbital dynamics. For the spacecraft simulator that drives the manipulator, parameters are selected as $I = \text{diag}\begin{bmatrix}4 & 8 & 5\end{bmatrix}$ kgm^2 and $\rho_t = \begin{bmatrix}-0.15 & 0 & 0\end{bmatrix}^T$ m. In order to be able to evaluate the accuracy of the estimated and predicted poses, the trajectory of the actual pose is also calculated directly by making use of the manipulator kinematics.

Figs. 8 and 9 show the trajectories of the estimated angular velocities and the inertial parameters, respectively. It is evident from the graphs that the estimator converges after about 60s. The trajectories of the pose prediction computed from the estimated sates and parameters versus the actual pose are plotted in Fig. 10, while the corresponding pose errors are illustrated in Fig. 11.

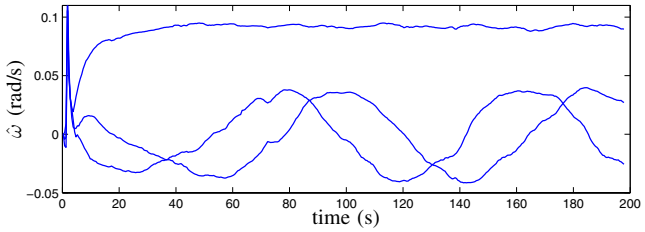

Fig. 8. Estimated angular velocities

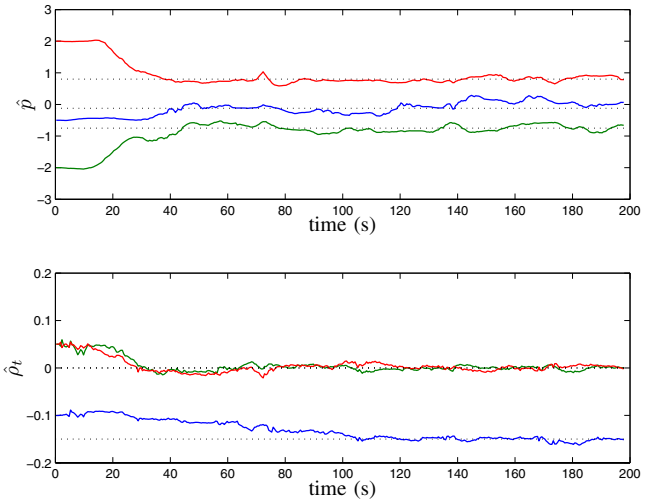

Fig. 9. Convergence of the estimated parameters to their true values

VII. Conclusion

A discrete-time adaptive estimator was developed for estimating the relative pose of two free-falling satellites that move in close orbits near each other using position and orientation data provided by a laser vision system. The adaptive estimator was able to tune itself to cope with uncertainty in the variance of the measurement noise and the inertial parameters of the target satellite. The covariance matrix of the measurement noise was modeled in a state-dependant form. This model allows additive quaternion noise, while preserving the unit-norm property of the quaternion. The effects of orbital mechanics was incorporated in the model-based estimator for both the accurate estimation and the prediction of the relative motion. The discrete-time model, including the state-transition matrix and the covariance of the process noise were derived in closed form suitable for

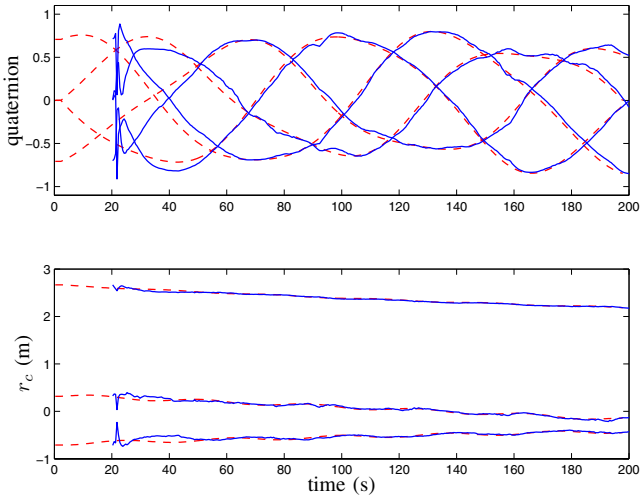

Fig. 10. Predicted pose (solid lines) verse the actual (dashed lines)

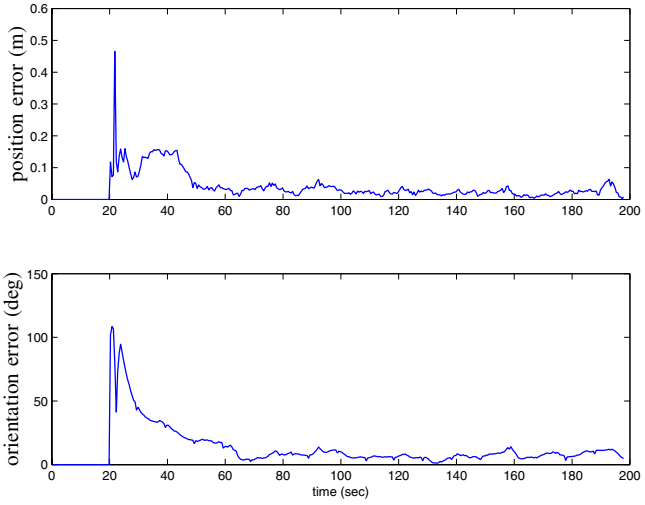

Fig. 11. The 20s-ahead pose-prediction errors

implementing the extended Kalman filter in real time. Also, we showed that the translational and rotational measurements are coupled and subsequently derived the corresponding observation matrix. Both simulation and experimental results were reported. The results demonstrated that the filer could accurately estimate and predict the states, parameters, and the covariance of the camera noise.

APPENDIX

Since A is a 3×3 matrix, its exponential can be computed from a second-degree polynomial:

$$e^{At} = a_0 I + a_1 A + a_2 A^2.$$

Moreover, the exponential of the eigenvalues of the matrix must satisfy

$$e^{\lambda_i t} = a_0(t) + a_1(t)\lambda_i + a_2(t)\lambda_i^2, \quad \text{for} \quad i = 1,2,3. \quad (32)$$

Therefore, if the eigenvalues are distinct, the coefficients of the polynomial can be found by solving the following linear system:

$$\begin{bmatrix} 1 & \lambda_1 & \lambda_1^2 \\ 1 & \lambda_2 & \lambda_2^2 \\ 1 & \lambda_3 & \lambda_3^2 \end{bmatrix} \begin{bmatrix} a_0 \\ a_1 \\ a_2 \end{bmatrix} = \begin{bmatrix} e^{\lambda_1 t} \\ e^{\lambda_2 t} \\ e^{\lambda_3 t} \end{bmatrix}. \quad (33)$$

That is

$$a_{k-1}(t) = \sum_{j=1}^{3} \gamma_{kj}\, e^{\lambda_j t} \quad \text{for} \quad k = 1,2,3$$

where γ_{kj}s are the elements of the inverse matrix in (33).

REFERENCES

[1] D. Zimpfer and P. Spehar, "STS-71 Shuttle/MIR GNC mission overview," in *Advances in Astronautical Sciences, American Astronautical Society*, San Diego, CA, 1996, pp. 441–460.

[2] G. Visentin and D. L. Brown, "Robotics for geostationary satellite service," in *Robotics and Automation System*, vol. 23, 1998, pp. 45–51.

[3] M. Oda, "Space robot experiments on NASDA's ETS-VII satellite – preliminary overview of the experiment results," in *IEEE 1999 International Conference on Robotics and Automation (ICRA '99)*, Detroit, USA, 1999, pp. 1390–1395.

[4] H. Ueno and et al., "Space robotic mission concepts for capturing stray objects," in *Proc. 7th Int. Symp. on Space Technology and Science*, Japan, June 2002.

[5] E. Bornschlegl, G. Hirzinger, M. Maurette, R. Mugunolo, and G. Visentin, "Space robotics in Europe, a compendium," in *Proc. 7th Int. Symp. on Artificial Intelligece, Robotics, and Automation in Space: i-SAIRAS 2003*, Japan, May 2003.

[6] K. Yoshida, "Engineering test satellite VII flight experiment for space robot dynamics and control: Theories on laboratory test beds ten years ago, now in orbit," *The Int. Journal of Robortics Research*, vol. 22, no. 5, pp. 321–335, 2003.

[7] C. Samson, C. English, A. Deslauriers, I. Christie, F. Blais, and F. Ferrie, "Neptec 3D laser camera system: From space mision STS-105 to terrestrial applications," *Canadian Aeronautics and Space Journal*, 2004.

[8] M. D. Lichter and S. Dubowsky, "State, shape, and parameter esitmation of space object from range images," in *IEEE Int. Conf. On Robotics & Automation*, New Orleans, April 2004, pp. 2974–2979.

[9] U. Hillenbrand and R. Lampariello, "Motion and parameter estimation of a free-floating space object from range data for motion prediction," in *The 8th Int. Symposium on Artifial Intelligent, Robotics and Automation in Space*, September, August 2005.

[10] Y. Masutani, T. Iwatsu, and F. Miyazaki, "Motion estimation of unknown rigid body under no external forces and moments," in *IEEE Int. Conf. on Robotics & Automation*, San Diego, May 1994.

[11] M. H. Kaplan, *Modern Spacecraft Dynamics and Control*. New York: Wiley, 1976.

[12] J. C. Wilcox, "A new algorithm for strapped-down inertial navigation," *IEEE Trans. on Aerospace and Electronic Systems*, vol. 3, pp. 796–802, Sept. 1967.

[13] E. J. Lefferts, F. L. Markley, and M. D. Shuster, "Kalman filtering for spacecraft attitude estimation," *Journal of Guidance*, vol. 5, no. 5, pp. 417–429, September–October 1982.

[14] M. E. Pittelkau, "Kalman filtering for spacecraft system alignment calibration," *Journal of Guidance, Control, and Dynamics*, vol. 24, no. 6, pp. 1187–1195, November 2001.

[15] J. Breakwell and R. Roberson, "Oribtal and attitude dynamics," *Lecture notes*, 1970.

[16] C. K. Chui and G. Chen, *Kalman Filtering with Real-Time Applications*. Berlin: Springer, 1998.

[17] R. K. Mehra, "On the identification of variances and adaptive kalman filtering," *IEEE Trans. on Automatic Control*, vol. 15, pp. 175–184, 1970.